An attempt towards ferrochromium production using molten oxide electrolysis

J. Biswas[1], L. Klemettinen[2], D. Sukhomlinov[3], W. Malan[4] and D. Lindberg[5]

1. Assistant Professor, IIT Bombay, Powai, Mumbai, Maharashtra 400076, India.
Email: biswasj@iitb.ac.in
2. Staff Scientist, Aalto University, Espoo, 00076 Aalto, Finland.
Email: lassi.klemettinen@aalto.fi
3. Post-doctoral researcher, Aalto University, Espoo, 00076 Aalto, Finland.
Email: dmitry.sukhomlinov@aalto.fi
4. Post-doctoral researcher, Aalto University, Espoo, 00076 Aalto, Finland.
Email: willem.malan@aalto.fi
5. Associate Professor, Aalto University, Espoo, 00076 Aalto, Finland.
Email: daniel.k.lindberg@aalto.fi

Keywords: MOE, FeCr, electrode, electrolyte, CO_2 emission reduction

ABSTRACT

In order to mitigate the effects of climate change, our society must be able to drastically reduce its CO_2 emissions. As the metallurgical industry is a considerable contributor to these emissions, new greener technologies must be invented and developed. One option could be the direct production of metals from oxides using renewable electricity.

The aim of this study was to investigate the possibility of using high-temperature molten oxide electrolysis (MOE) for iron and ferrochrome production. FactSage was utilised for estimating a feasible equilibrium electrolyte composition, and the experiments were conducted at 1550-1580 °C in conical alumina crucibles with iridium wire as the cathode and platinum wire as the anode. The sources of iron and chromium were either pure FeO powder or industrial chromite pellets. Voltage was applied to the electrolysis cell for 6 hours and the resulting current was measured, along with oxygen concentration in the off-gas line.

The electrolyte comprised of SiO_2, Al_2O_3, MgO and CaO. First, the effect of FeO concentration on iron reduction efficiency was investigated using only pure oxide powders as starting materials. The results indicated that 10 wt% FeO mixed with the electrolyte resulted in more efficient iron reduction compared to 20 wt%. In further experiments, industrial chromite pellets were ground and mixed with the CaO-free electrolyte. Iron and chromium reduction efficiencies were higher when approximately 19 wt% of the total sample mass consisted of pellets compared to increasing the pellet amount to 37 wt%. Generally, the chromium solubility in the liquid electrolyte was relatively low, and most of the chromium was confined to the spinel solid solution, from where its dissolution to the liquid electrolyte was very slow, resulting in slow reduction kinetics. For larger scale applications, economically more viable electrode materials should be investigated.

INTRODUCTION

The global challenge to mitigate the greenhouse gas emission has impacted steel industry, which accounts for 7 to 9% of global greenhouse gas emissions (Kim *et al,* 2022). The traditional iron production process involves coke for iron ore reduction, resulting in a carbon footprint of 1.6 – 2 tons of CO_2 per ton of crude steel (Somers, 2021). Currently, EU aims to decrease the greenhouse gas emissions by 80-95% by 2050 compared to the level in 1990 (European Commission, 2011), which will also require a technological breakthrough in the steel industry. In order to address this challenge, extensive research is ongoing globally for example regarding hydrogen steelmaking (Patisson and Mirgaux, 2020), carbon capture & storage (Raza *et al,* 2019) and molten oxide electrolysis (Allanore, 2015). Molten oxide electrolysis (MOE) is a process where metals can be produced directly by electrolysis of oxidic ores or concentrates (Allanore, 2015). In recent years, this technology has drawn the attention of several steelmakers as a possible clean metals production route. The main challenges in iron ore electrolysis can be summarised as 1) the operating temperature should be above the melting temperature of iron (1538 °C), 2) most metals that could be used as anodes do not survive under the corrosive and oxidising conditions at the anode, 3) the multivalent state of iron causes loss of current due to electronic conduction in the melt (Allanore, Yin and Sadoway, 2013).

In recent years, there has been some progress about anode materials and more information has been obtained regarding the electrochemical nature of iron ions in oxide melts (Zhou *et al,* 2017). Initially, Kim *et al,* (2011) proposed iridium as an anode material, but only for acidic melts. Later, Allanore, Yin and Sadoway (2013) proposed a chromium-based alloy for anode, which exhibited limited consumption during iron extraction and oxygen evolution due to formation of an electronically conductive solid solution of chromium and aluminium oxide. Wiencke *et al,* (2018) studied production of iron from acidic melt by electrolysis, utilising platinum as anode and an alloy of platinum and 30% rhodium as cathode. In another work, Zhou *et al,* (2017a) produced Fe and Fe-Ni alloys from CaO-MgO-SiO_2-Al_2O_3-Fe_2O_3 and CaO-MgO-SiO_2-Al_2O_3-Fe_2O_3-NiO melts using a graphite anode and molybdenum cathode. Jiao *et al,* (2018) produced Ti-Fe alloys via MOE from CaO-Al_2O_3-MgO-TiO_2 melt using liquid iron as cathode and graphite as anode. Liu, Zhang and Chou (2015) have also demonstrated iron production from CaO-Al_2O_3-SiO_2-Fe_2O_3 melt via electrolysis using molybdenum cathode and graphite anode. Although some progress has been made, the technology is still facing several other challenges, such as low current efficiency and lack of inexpensive, inert anode materials. The use of graphite as an anode is feasible, but as the oxygen formed at the anode reacts

with carbon, some direct CO_2 emissions will be produced. More research is required to mature this technology for industrial iron production without any direct CO_2 emissions.

In this study, a set-up for molten oxide electrolysis experiments was established and experiments were conducted with synthetic MgO-SiO_2-Al_2O_3-CaO-FeO mixtures to produce molten iron by electrolysis. Some experiments were also conducted with industrial chromite pellets, with an objective to test the feasibility of producing ferrochrome alloy via molten oxide electrolysis in laboratory scale.

EXPERIMENTAL

Materials

The raw materials for the study were synthetic oxide powders and industrial chromite pellets supplied by Outokumpu (Finland), as presented in Tables 1 and 2. For each experiment, a total of approximately 16 g of the oxide mixture was prepared by grinding the oxides at different mass ratios using mortar and pestle, followed by pressing the mixtures into pellets. The starting compositions for all four experiments presented in this work are shown in Table 3.

TABLE 1 - Materials used in the experiments.

Material	Supplier	Purity	Notes
Al_2O_3	Sigma Aldrich	> 99%	
SiO_2	Sigma Aldrich	99%	
MgO	Sigma Aldrich	> 99%	
CaO	Sigma Aldrich	99.9%	
FeO	Sigma Aldrich	99.7%	
Chromite pellets	Outokumpu, Finland	See Table 2 below	From Kemi mine, diameter approx. 10 mm
Pt (anode and wiring)	Johnson-Matthey Noble Metals	> 99.9%	Diameter 0.5 mm (anode) and 0.25 mm (wires)
Ir (cathode)	Johnson-Matthey Noble Metals	> 99.9%	Diameter 0.5 mm
Al_2O_3 (crucible)	Kyocera	> 99.5%	Conical, max diameter 29 mm, height 38 mm
Al_2O_3 (tubes)	Kyocera	> 99.5%	OD 8 mm (supporting rod), OD 1 mm (electrode & wiring protection)
Al_2O_3 cement (two-component)	Morgan Advanced Materials Haldenwanger GmbH		Used for building the supporting rod and attaching electrodes

TABLE 2 - Composition of chromite pellets.

	SiO_2	Al_2O_3	MgO	Fe_2O_3	FeO	Cr_2O_3	MnO	TiO_2	CaO
wt%	3.3	13.8	11.2	23.8	2.9	43.8	0.20	0.50	0.6

TABLE 3 - Starting compositions for the experiments, in wt%.

Oxide melt code	Al_2O_3	SiO_2	MgO	FeO	Fe_2O_3	Cr_2O_3	CaO	MnO	TiO_2
A	20.0	48.0	12.0	10.0			10.0		
B	17.5	42.0	10.5	20.0			10.0		
C	18.5	31.8	23.8	1.0	8.5	15.7	0.2	0.07	0.18
D	19.9	39.7	27.3	0.5	4.3	7.9	0.1	0.04	0.09

Apparatus

A vertical laboratory furnace (Nabertherm RHTV 120-150/18, equipped with molybdenum disilicide heating elements) with 38 mm inner diameter alumina work tube was used for the experiments. The furnace gas outlet was connected to an oxygen sensor (Rapidox 2100ZF) for the measurement of the oxygen concentration using Rapidox software. The furnace was also connected to a potentiostat-galvanostat (VersaSTAT 4, Princeton Applied Research) for the application of potential and VersaStudio software was used for recording the data. The electrolysis cell consisted of a conical alumina crucible of 29 mm max diameter and 38 mm outer height, and the final design used an iridium wire cathode of 0.5 mm diameter and a platinum wire anode of 0.5 mm diameter. Trials were conducted using thinner electrode wires, which resulted in the wires breaking during the experiments. Similar problems were also encountered when iridium was tested as the anode.

The electrodes were immersed from the top of the crucible and secured with alumina cement at approximately diametric opposite locations (Figure 1). The cathode wire was placed at the bottom of the electrolysis cell, and the vertical part was covered by a thin alumina tube. The anode was placed on the other side of the cell, approximately 12 mm above the bottom of the cell. At the beginning of each experiment, the distance from the tip of the cathode to the tip of the anode was approximately 12 mm. To hold the electrolysis cell, a bigger cylindrical crucible (35 mm outer diameter and 50 mm height) was connected to a hollow supporting rod. The anode and cathode wires from the cell were welded to the electrical wires (0.25 mm diameter platinum) and passed through the supporting rod to the outside of the furnace and connected to the potentiostat. One of the electrical wires within the supporting rod was covered by a thin alumina rod, to avoid any possibility of a short circuit.

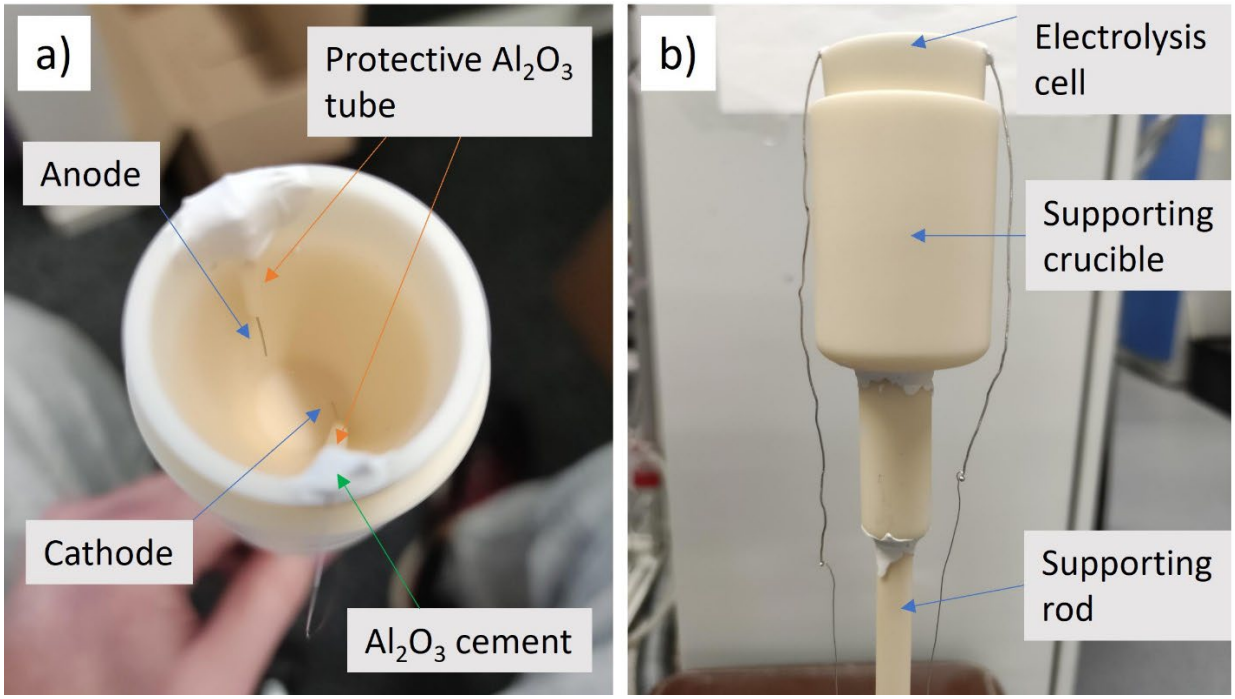

FIG 1 - (a) Electrolysis cell from the top, showing the cathode and anode, (b) Electrolysis cell inside the supporting crucible, attached to the supporting rod.

Procedure

For the experiments, the electrolysis cell with the oxide mixture was first lifted to the middle of the furnace at room temperature using the support rod, after which the furnace was sealed. The furnace was heated to the target temperature at 4 °C/min under continuous flow of argon with 120 ml/min flow rate. The oxygen measurement was started approximately 30 minutes after starting to heat the furnace, and the measurement interval was 10 seconds. At the target temperature, the experiments were conducted in potentiostatic mode of the potentiostat-galvanostat, i.e. a constant potential was applied to the cell for a certain period of time and the resulting electrical current data was recorded every 5 seconds. After the completion of the experiment, the furnace was cooled to room temperature under argon atmosphere, after which the cell was removed from the furnace, the sample was collected and broken using a hammer, and the weight of the formed metal alloy droplet at the cathode was recorded.

Characterisation

The preliminary elemental compositions of the metal alloys, slags and spinels were analysed using a scanning electron microscope (SEM, Mira3, Tescan, Czech Republic) equipped with an energy dispersive spectrometer (UltraDry Silicon Drift EDS, Thermo Fisher Scientific, USA). The final chemical compositions of all three phases were characterised using EPMA (SX100, Cameca SAS, France) with 20 kV acceleration voltage and 40 nA beam current. Depending on the phase, either focused, 5 µm or 20 µm defocused beam diameters were employed. The used standards as well as X-ray lines analysed and peak & background dwell times have been presented in Table 4. The elements Mn and Ti were present only in trace quantities and originated from the industrial chromite pellets.

TABLE 4 - EPMA parameters: analysed elements, X-ray lines, peak & background dwell times and standard materials utilised.

Element	**O**	**Si**	**Al**	**Cr**	**Mg**	**Ir**	**Pt**	**Ca**	**Mn**	**Fe**	**Ti**
Line	Kα	Kα	Kα	Kα	Kα	Lα	Lα	Kα	Kα	Kα	Kα
Peak dwell time (s)	20	20	20	30	20	20	30	20	20	20	20
Total background dwell time	20	20	20	30	20	20	30	20	20	20	20
Standard material	Al_2O_3	Quartz	Al_2O_3	Chro-mite	Diop-side	Ir metal	Pt metal	Diop-side	Rhodo-nite	Hema-tite	Rutile

RESULTS & DISCUSSION

Electrolysis for iron production

The first electrolysis experiment for iron oxide reduction was performed in potentiostatic mode with 10% CaO, 12% MgO, 48% SiO_2, 20% Al_2O_3, 10% FeO (melt A) at 1540 °C. The phase diagrams for the melt, in two oxygen partial pressures at 1550 °C, are presented in Figure 2. In a molten oxide electrolysis cell, oxygen pressure at the anode increases due to oxygen evolution reaction. The slag composition for this experiment was selected in the fully liquid region as marked in Figure 2. When the oxygen partial pressure increases during electrolysis, the slag should still remain fully liquid throughout the electrolysis cell, according to Figure 2 b.

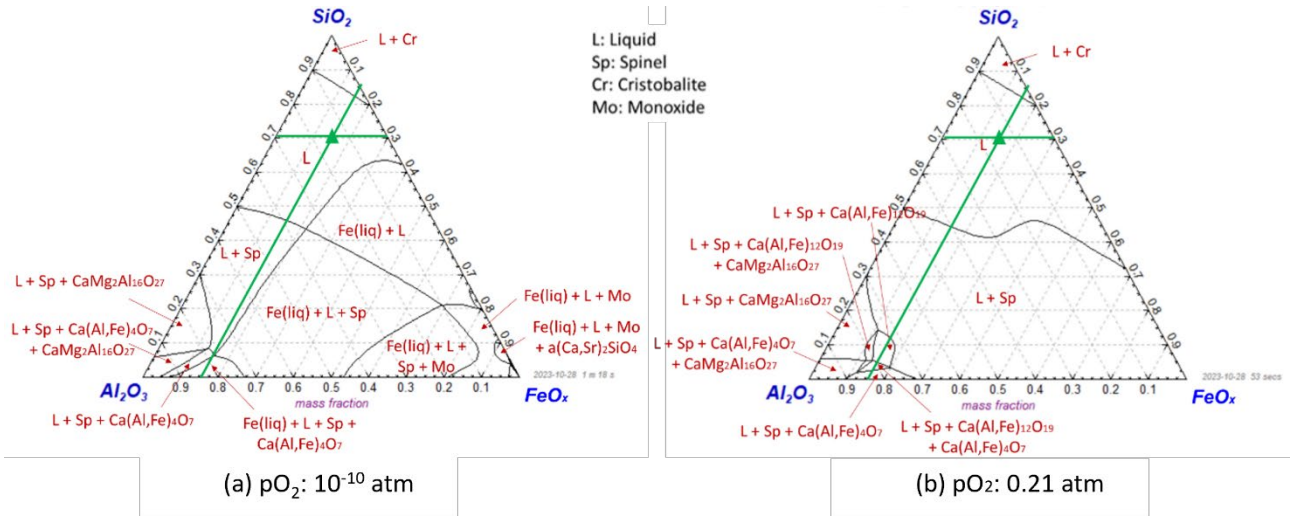

FIG 2 - SiO_2-Al_2O_3-FeO_x ternary phase diagrams at 1550 °C with fixed CaO and MgO concentrations (10 wt% each) at oxygen partial pressure of 10^{-10} and 0.21 atm in (a) and (b), respectively. The green triangle represents the starting composition in the first experiment (melt A). The lower oxygen partial pressure represents the area around the cathode and the higher represents the area around the anode.

A potential of 3V was applied to the oxide melt for 6 hours. The resulting electrical current and the oxygen concentration in the off-gas line as a function of time have been presented in Figure 3. For the experiments where only iron oxide reduction occurred, 3V potential was chosen in order to imitate the experimental conditions chosen by Wiencke *et al,* (2018).

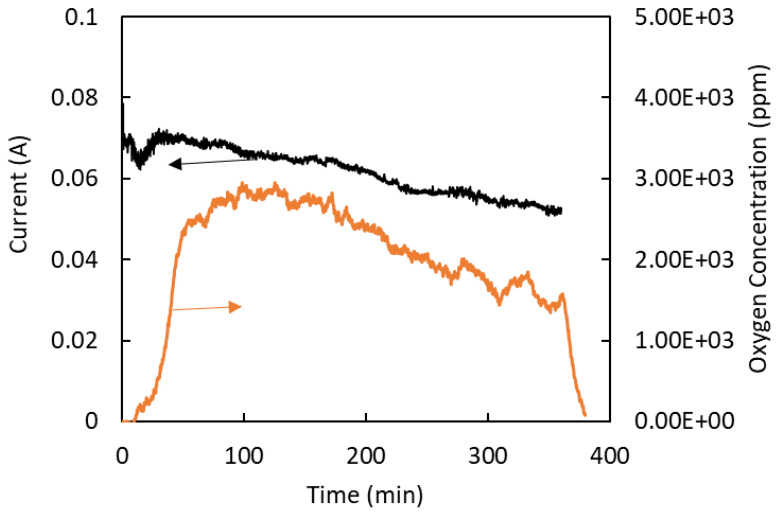

FIG 3 - Current in the electrolysis cell (black line) and oxygen concentration (orange line) as a function of time for electrolysis of 10% CaO, 12% MgO, 48% SiO_2, 10% Al_2O_3, 10% FeO melt at 1540 °C with 3V potential.

Initially, the current through the cell was approximately 80 mA and it decreased with the progression of reduction, reaching a value of slightly over 50 mA at the end of the 6-hour experiment. Previous studies on electrical properties of FeO-CaO, FeO-SiO_2, CaO-SiO_2 and CaO-FeO-SiO_2 slags/melts have revealed that cations (such as Ca^{2+} or Fe^{2+} ions) are the exclusive ionic charge carriers in these melts and contribute significantly to the ionic conductivity (Barati and Coley, 2006a and 2006b). Other ions, such as $(SiO_4)^{4-}$ and $(FeO_4)^{5-}$ are relatively immobile due to their large tetrahedral structures, hence their contribution to ionic conductivity can be ignored. Therefore, for CaO-MgO-SiO_2-Al_2O_3-FeO melt, it can be assumed that ionic conduction happens through only Ca^{2+}, Fe^{2+} and Mg^{2+} ions. As the electrolysis time increases, the concentration of Fe^{2+} ions decreases in the melt due to reduction into metallic iron, which in turn decreases the ionic conductivity of the melt. This is in agreement with observations from electrolysis in aqueous medium (Yuan and Haarberg, 2009; King and Botte, 2011), and is the reason for the slow decrease in the measured current value with

time in Figure 3. The corresponding oxygen concentration could be seen to increase to as high as approximately 2750 ppm during the electrolysis. It could also be noted that there exist few small peaks, indicating fluctuations and sudden rises in the oxygen concentration. Generally, these oxide melts are viscous, which may cause difficulties in releasing the generated oxygen bubbles from the anode. There is a possibility of a fraction of the anode surface area being blocked by oxygen bubbles, which would decrease the available surface area for further anodic reactions. The sudden release of these bubbles from anode possibly results in sudden rises in oxygen concentrations (small peaks at different times). This phenomenon at the anode has also been reported by Zhou *et al*, (2017b).

After 6 hours of electrolysis for this melt, a metal droplet weighing 0.14 g was recovered at the cathode and the composition of this metal alloy droplet was 79.1 wt% Fe and 20.4 wt% Ir according to EPMA analysis. An SEM image of the metal droplet is shown in Figure 4 b. Even though a significant amount of Ir dissolved in the metal alloy droplet, the cathode retained roughly its original shape after several hours of electrolysis. An image of the electrolyte, showing spinel formation at the crucible-electrolyte interface and within the electrolyte, is shown in Figure 4 a.

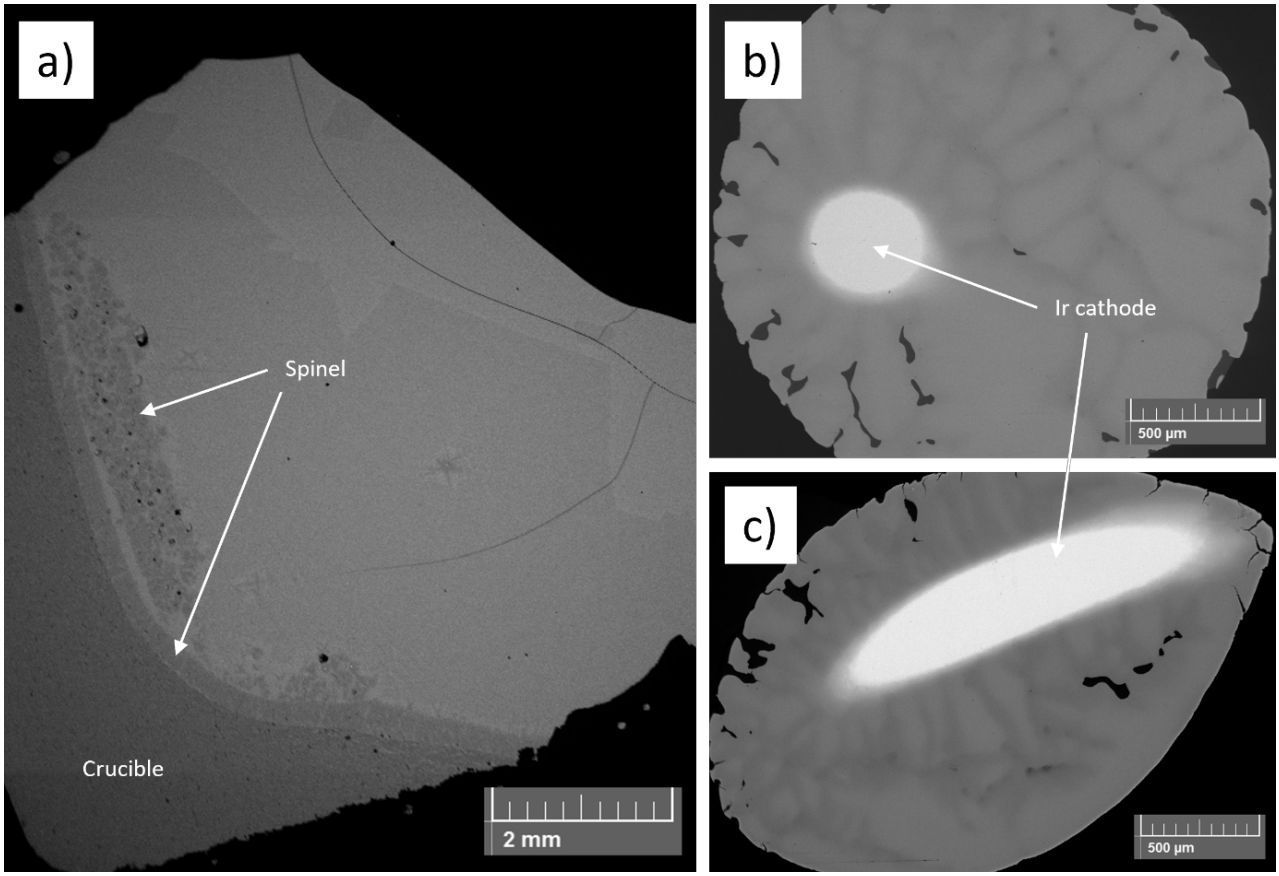

FIG 4 - a) Microstructure of the electrolyte (slag) after FeO reduction with 10 wt% FeO and 10 wt% CaO (melt A); b) metal alloy droplet formed during the experiment with 10 wt% FeO and 10 wt% CaO; c) metal alloy formed during the experiment with 20 wt% FeO and 10 wt% CaO (melt B). 3V potential was applied in all cases.

The cathodic efficiency was calculated according to Equation (1) from the iron recovered at the cathode and the total transferred charge from the cathode, assuming all charge transfer was due to the cathodic reaction of iron oxide reduction.

$$Cathodic\ efficiency = \frac{Fe_{recovered}}{Fe_{current}} * 100\% \quad (1)$$

where $Fe_{recovered}$ is the total moles of iron recovered from the cell and $Fe_{current}$ is the moles of Fe generation expected based on the cell current, assuming all charge is involved in iron reduction.

The results from the current study were compared with the results obtained by Wiencke *et al,* (2018). They performed electrolysis by applying 3V potential for 6 hours on 15% FeO, 17% Al_2O_3, 56.1%

SiO_2, 11.9% MgO melt at 1550 °C. Interestingly, the current in their electrolysis cell seemed to increase from 70 mA to around 80 mA, whereas in our case, the current decreased with time. Wiencke *et al* obtained a cathodic efficiency of 36%, which is quite comparable with the value of 27.6% obtained in the current study.

To gain a better understanding of the iron reduction process with MOE, another experiment was conducted using a higher FeO starting concentration (20 wt%, melt B). The iron oxide concentrations of 10 and 20 wt% in this work were chosen based on the work of Sadoway (1995). A potential of 3 V was applied for 6 hours, and the formed metal alloy droplet is shown in Figure 4 c. Interestingly, the cell current almost doubles (from 70 mA to 118 mA) by doubling the Fe-ion concentration in the melt, as presented in Figure 5. The cathodic efficiencies for the experiments with 10 and 20 wt% FeO were calculated according to Equation (1). Table 5 presents the viscosities from Factsage, cathodic efficiencies, as well as ionic and electronic conductivities for both melts. The ionic conductivities were calculated from Nernst Einstein Equation (Barati and Coley, 2006b), where cations Ca^{2+}, Fe^{2+} and Mg^{2+} were assumed to be the exclusive ionic charge carriers. For this calculation, the diffusivities of Ca^{2+} and Fe^{2+} were adopted from the values reported by Barati and Coley (2006b) and modified according to the respective slag viscosities. As the data for Mg^{2+} diffusivity was not available, it was assumed to be the same as Ca^{2+}. The electronic conductivities of the melts were calculated based on the diffusion assisted charge transfer model developed by Barati and Coley (2006b). Both ionic and electronic conductivities in the melt increase with total Fe-ion concentration increase. This illustrates the reason for higher cell current with higher FeO concentration. Although the cell current rises with increasing FeO concentration, the cathodic efficiency decreases and the Fe recovery from melt also decreases, indicating very poor performance with the melt containing more iron oxide. According to Table 5, the ionic conductivity increases by 33% with increasing total FeO concentration from 10% to 20%, while at the same time the electronic conductivity increases by 470%. The higher electronic conductivity increases cell current losses, and this possibly results in lower cathodic efficiency and decreased Fe recovery from electrolysis of higher iron oxide melt. On the other hand, FeO being a network breaker, viscosity decreases with increasing iron oxide concentration, which should ease the escape of O_2 bubbles from the melt. It should also be noted that the electrolysis cell broke towards the end of the experiment with 20 wt% FeO (current decrease after 300 min in Figure 5), resulting in some of the electrolyte leaking to the support crucible. This also has some contribution to the poor reduction performance. The breakage was most likely due to significant alumina dissolution from the crucible (electrolysis cell) because the starting composition of the electrolyte was relatively far from the liquid-spinel saturation boundary shown in the phase diagrams of Figure 2.

The overall Fe recovery percentage was calculated based on Equation (2),

$$Fe\ Recovery\ (\%) = \frac{Fe_{recovered}}{Fe_{total}} * 100\% \qquad (2)$$

where Fe_{total} is the total moles of Fe in the oxide melt at the beginning of the experiment. The iron recovery was approximately 9.2% with 10 wt% FeO in the starting mixture and decreased to 3.4% when FeO concentration was increased to 20 wt%. These values are very low compared to the traditional ironmaking processes.

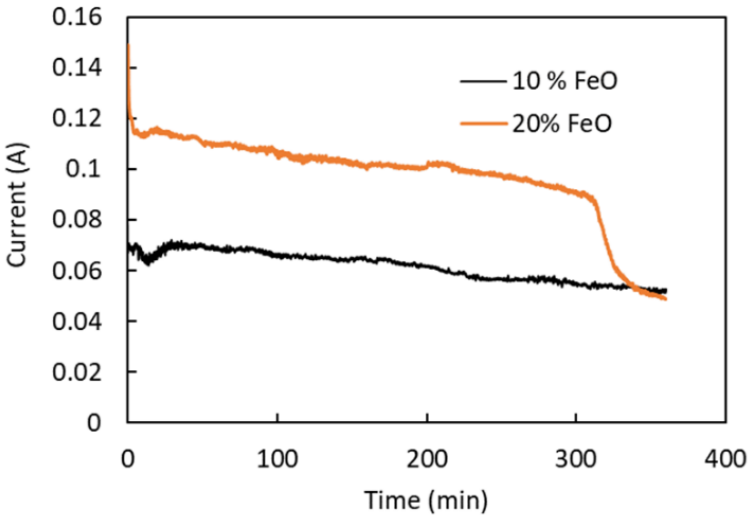

FIG 5 - Cell current profile for electrolysis of CaO-SiO_2-Al_2O_3-MgO-FeO melts with two different concentrations of FeO at 1540 °C.

TABLE 5 - Comparison of CaO-SiO_2-Al_2O_3-MgO-FeO melt electrolysis performance at 1540 °C with 3V potential by varying the FeO concentration.

Oxide melt code	Electrolyte FeO (wt%)	Viscosity (Poise)	Cathodic Efficiency (%)	Electronic Conductivity (S/m)	Ionic Conductivity (S/m)	Fe Recovery (%)
A	10	9.30	27.6	0.03	18.62	9.15
B	20	3.36	13.1	0.17	24.86	3.43

Electrolysis for ferrochrome production

The feasibility of MOE for ferrochrome production was also investigated with two experiments. The electrolyte consisted of Al_2O_3-SiO_2-MgO mixed with chromite pellets (Table 2) at different mass ratios. Two phase diagrams for the pellet-containing system are presented in Figure 6 at 1550 °C for $pO_2 = 10^{-10}$ and 0.21 atm. The green triangle represents the starting composition for the experiment with melt C (Table 3). The single-phase liquid region almost disappears when the oxygen pressure increases from 10^{-10} atm to 0.21 atm, indicating that with any melt composition, there will always be spinels present near the anode, i.e. high oxygen partial pressure region. In this case, when using chromite pellets in the starting mixture, the composition will always be in the liquid-spinel region. This means that the melt viscosity will increase, but the alumina crucible dissolution will decrease, increasing the lifetime of the electrolysis cell.

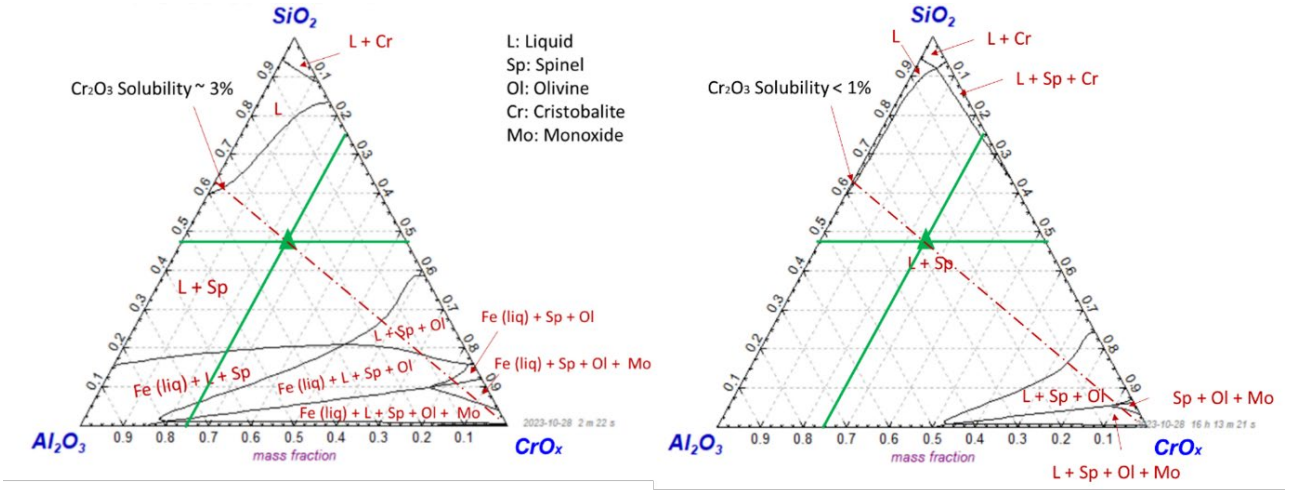

FIG 6 - SiO_2-Al_2O_3-CrO_x ternary phase diagrams at 1550 °C with MgO, Fe_2O_3 and CaO concentrations fixed at 23.8 wt%, 9.71 wt% and 0.21 wt%, respectively, for oxygen partial pressures of 10^{-10} and 0.21 atm.

The first experiment with chromite pellets was performed at approximately 1580 °C with 5.8 g of pellets, resulting in 8.5 wt% Fe_2O_3, 1.0 wt% FeO and 15.7 wt% Cr_2O_3 in the melt (oxide melt C in Table 3). As the reduction potential of chromium is higher than that of iron, a higher cell potential was selected for this case. A potential of 6V was applied for 6 hours, and a metal droplet of approximately 0.45 g (64.5 wt% Fe, 2.4 wt% Cr and 32.6 wt% Ir according to EPMA analyses) was reduced at the cathode. The cell current profile as well as the oxygen concentration profile are presented in Figure 7, and the formed metal alloy droplet is shown in Figure 8 b. The cell current slowly increases during the first 100 minutes, after which it remains stable for about 150 minutes and then it decreases. The oxygen evolution profile shows almost similar trend, but with few additional peaks. Interestingly, the cell current for electrolysis of synthetic iron oxide, as presented in Figures 3 and 5, was observed to decrease continuously as a function of time. In the synthetic iron oxide case, all the conducting ions (Ca^{2+}, Mg^{2+}, Fe^{2+}) were more or less uniformly distributed in the liquid oxide, where the concentration of Fe^{2+} ions decreased due to reduction, and this resulted in decreasing ionic conductivity with increasing electrolysis time. In contrast to that, for the oxide system with pellets, a large amount of the conducting ions are expected to be bound inside the solid spinel phase (Figure 6 and Figure 8 a). These ions (Cr^{3+}, $Fe^{3+,2+}$, Mg^{2+}) slowly dissolve to the liquid electrolyte, maintaining its composition almost the same during the electrolysis process. Therefore, the conductivity variation over time should be lower in this case, resulting in a relatively stable cell current. The peaks in oxygen profile could be due to sudden escape of O_2 bubble clusters from the anode. However, these peaks are more prominent during chromite pellet reduction compared to synthetic FeO reduction. Oxygen evolution in molten oxides is likely controlled by the oxygen-containing reactant transport (Allanore, 2013), and some explanations may be found from spatiotemporal differences in transport properties of the melts during the electrolysis process.

The recoveries of Fe and Cr, according to Equation (2), were calculated to be 26.4% and 0.6%, respectively. Although the iron recovery is higher with chromite pellets compared to synthetic FeO reduction, the Cr recovery seems to be very low. The main challenge for chromium reduction is the low solubility of chromium oxide in the liquid electrolyte at the experimental temperature. The chromium reduction seems to be a three-step process: 1) chromium oxide dissolution from the spinel to the liquid phase, 2) transport of chromium ions in the liquid phase to the cathode, and 3) reduction of chromium ions at the cathode. Furthermore, chromium is a multivalent ion, therefore its reduction occurs firstly from 3+ to 2+, followed by reduction into metallic Cr at the cathode. It is unclear which stage is the rate limiting in this case, but the complexity of chromium reduction process is evident.

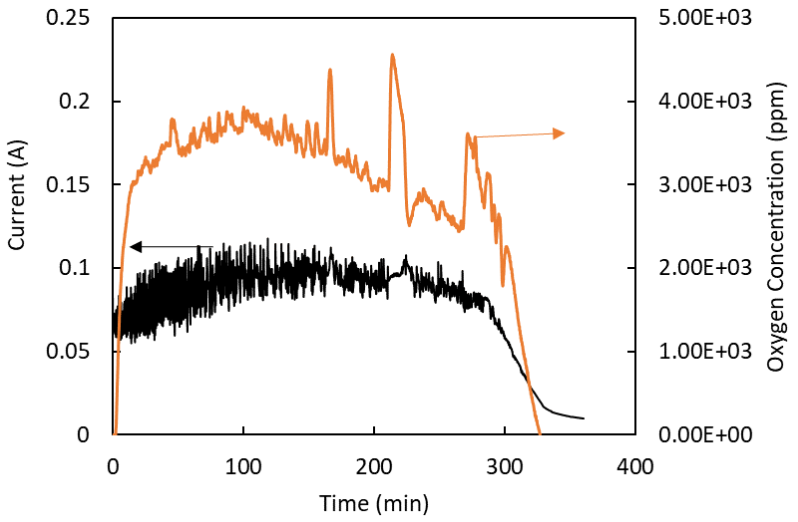

FIG 7 - Cell current (black line) and oxygen concentration (orange line) as a function of time for electrolysis of oxide melt C at 1580 °C with 6V cell potential.

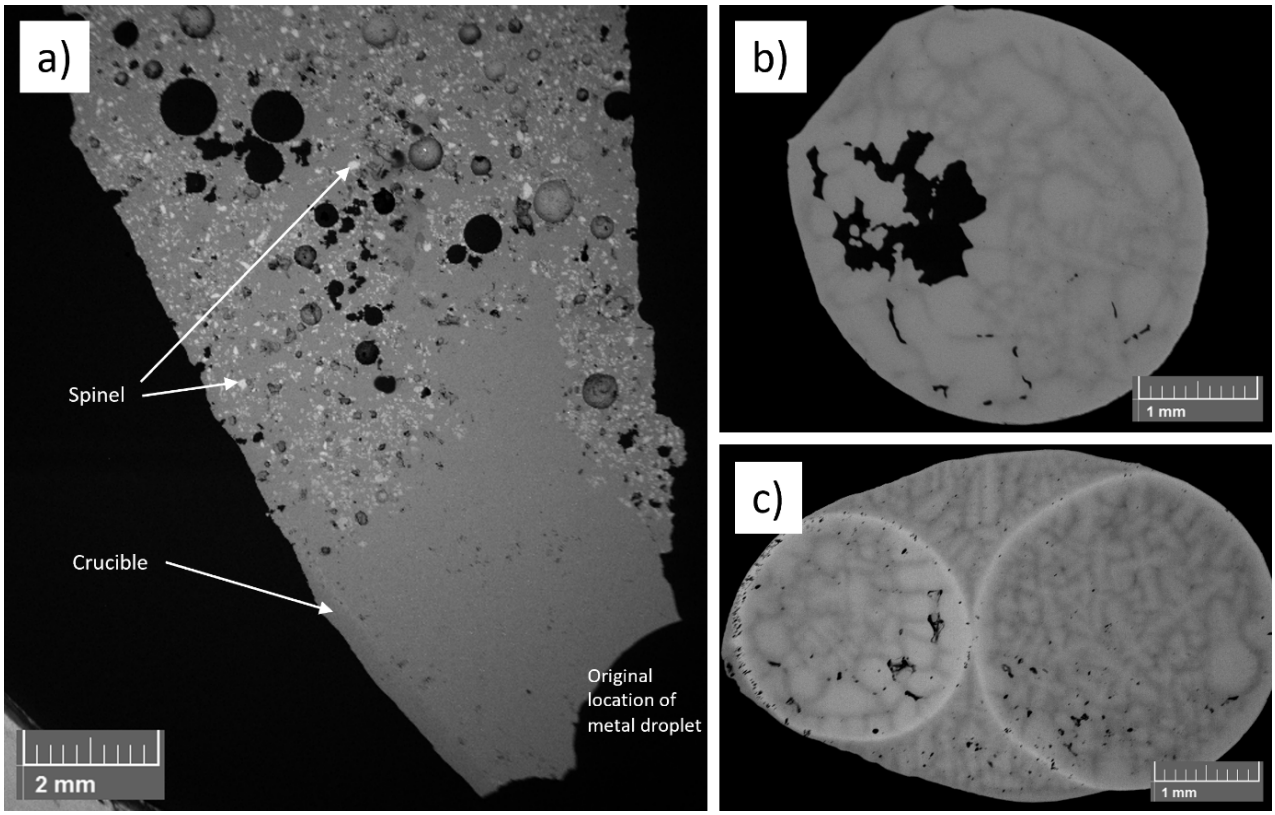

FIG 8 - a) Microstructure of the electrolyte (slag) after iron and chromium reduction from chromite pellets with melt D; b) metal alloy droplet formed during reduction with melt C; c) alloy formed during reduction with melt D. 6V potential was applied in all cases.

The second electrolysis experiment containing chromite pellets was conducted by decreasing the pellet mass (melt D). SEM images of the electrolyte and formed metal alloy are shown in Figure 8 a and c, respectively. Cell current profile comparison for melts C and D is presented in Figure 9 and the starting composition comparison is shown in Table 3. Interestingly, the cell current is much lower for the higher iron and chromium oxide containing melt compared to the melt with lower concentration of these oxides. The recovery of iron and chromium could also be observed to increase with decreasing pellet mass, as shown in Table 6. When decreasing the pellet mass, the starting composition is closer to the liquid phase boundary shown in Figure 6, indicating a lower fraction of spinel and lower total viscosity, which increases the mobility of the conducting ions and could explain the higher cell current as well as higher Fe and Cr recoveries.

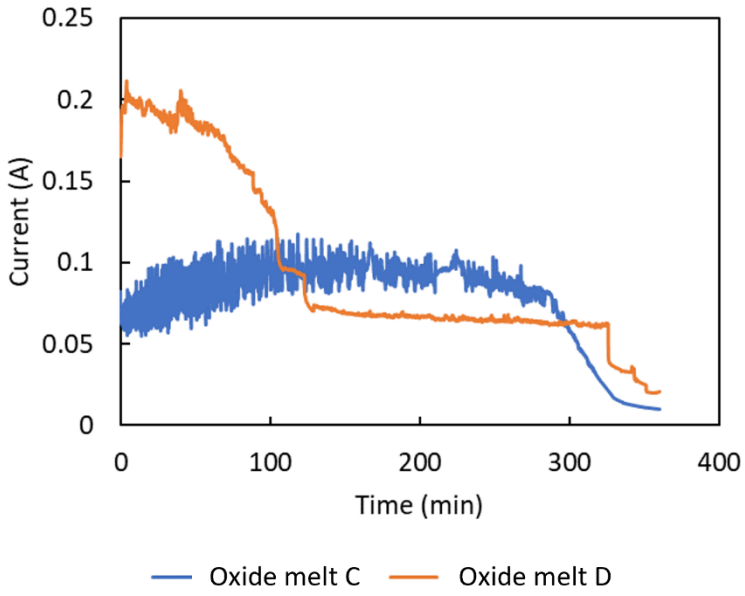

FIG 9 - Cell current profiles for electrolysis of CaO-SiO_2-Al_2O_3-MgO-Fe_2O_3-Cr_2O_3 melts with different masses of ferrochrome pellets at 1580 °C.

TABLE 6 - Electrolysis performance comparisons of ferrochrome containing oxide systems C and D at 1580 °C with 6V cell potential.

Oxide system code	Mass of pellets / total sample mass (g)	Viscosity (Poise)	Fe recovery (%)	Cr recovery (%)
C	5.8 / 16	Higher	26.4	0.62
D	3.0 / 16	Lower	30.9	1.77

According to Sadoway (1995), the MOE technology could be capable of producing ferrochromium (80% Fe – 20% Cr) with less energy than the existing processes, and naturally with considerably less process carbon. However, based on the results of the current study, a huge amount of work is required before ferrochromium production using MOE can be considered feasible and attractive.

CONCLUSIONS

In this study, the performance of molten oxide electrolysis for the reduction of iron oxide and chromite pellets was investigated. For CaO-SiO_2-Al_2O_3-MgO-FeO melt, the iron recovery was less than 10% and it decreased with increasing concentration of FeO from 10 to 20 wt% in the starting mixture. When adding industrial chromite pellets to the melt without CaO, the iron recovery improved significantly compared to synthetic iron oxide reduction. Decreasing the pellet mass from 5.8 g to 3 g (total mass approximately 16 g) resulted in a slight increase in iron recovery while chromium recovery almost tripled, however, it still remained below 2%.

Provided that green electricity is available, molten oxide electrolysis is a clean metal production technology and could be a potential route for larger iron production in the future. However, extensive research is required to make the process efficient enough for production of chromium-containing alloys, and in general to make the process industrially attractive.

ACKNOWLEDGEMENTS

This study is part of the Business Finland-funded TOCANEM Project (Grant number 2118452). During the work, the Academy of Finland's RawMatTERS Finland Infrastructure (RAMI) based at Aalto University, GTK, and VTT in Espoo was utilised.

REFERENCES

Allanore, A, 2013. Electrochemical engineering of anodic oxygen evolution in molten oxides. *Electrochimica Acta*, 110:587-592.

Allanore, A, 2015. Features and Challenges of Molten Oxide Electrolytes for Metal Extraction, *Journal of The Electrochemical Society*, 162(1):E13-E22.

Allanore, A, Yin, L and Sadoway, D, 2013. A new anode material for oxygen evolution in molten oxide electrolysis, *Nature*, 497:353–356.

Barati, M and Coley, K.S, 2006a. Electrical and Electronic Conductivity of $CaO\text{-}SiO_2\text{-}FeO_x$ Slags at Various Oxygen Potentials: Part I. Experimental Results, *Metallurgical & Materials Transactions B*, 37B:41-49.

Barati, M and Coley, K.S, 2006b. Electrical and Electronic Conductivity of $CaO\text{-}SiO_2\text{-}FeO_x$ Slags at Various Oxygen Potentials: Part II. Mechanism and a Model of Electronic Conduction, *Metallurgical & Materials Transactions B*, 37B:51-60.

European Commission, 2011. A Roadmap for Moving to a Competitive Low Carbon Economy in 2050. Available from: https://eur-lex.europa.eu/LexUriServ/LexUriServ.do?uri=COM:2011:0112:FIN:en:PDF (Accessed: 11 January 2024)

Jiao, H, Tian, D, Tu, J and Jiao, S, 2018. Production of Ti-Fe alloys via molten oxide electrolysis at a liquid iron cathode, *RSC Advances*, 8:17575-17581.

Kim, H, Paramore, J, Allanore, A and Sadoway, D.R, 2011. Electrolysis of Molten Iron Oxide with an Iridium Anode: The Role of Electrolyte Basicity, *Journal of The Electrochemical Society*, 158(10):E101-E105.

Kim, J, Sovacool, B.K, Bazilian, M, Griffiths, S, Lee, J, Yang, M and Lee, J, 2022. Decarbonizing the iron and steel industry: A systematic review of sociotechnical systems, technological innovations, and policy options, *Energy Research & Social Science*, 89:102565.

King, R.L and Botte, G.G, 2011. Hydrogen production via urea electrolysis using a gel electrolyte, *Journal of Power Sources*, 196(5):2773-2778.

Liu, J-H, Zhang, G-H and Chou, K-C, 2015. Electrolysis of Molten FeO_x-Containing $CaO\text{-}Al_2O_3\text{-}SiO_2$ Slags under Constant Current Field, *Journal of the Electrochemical Society*, 162(12):E314-E318.

Patisson, F and Mirgaux, O, 2020. Hydrogen Ironmaking: How It Works, *Metals*, 10:922.

Raza, A, Gholami, R, Rezaee, R, Rasouli, V and Rabiei, M, 2019. Significant aspects of carbon capture and storage – A review, *Petroleum*, 5(4):335-340.

Sadoway, D.R, 1995. New opportunities for metals extraction and waste treatment by electrochemical processing in molten salts. *Journal of Materials Research*, 10:487–492.

Somers, J, 2021. Technologies to decarbonise the EU steel industry, EUR 30982 EN, Publications Office of the European Union, Luxembourg, ISBN 978-92-76-47147-9 (online), doi:10.2760/069150 (online), JRC127468

Wiencke, J, Lavelaine, H, Panteix, PJ, Petitjean, C and Rapin, C, 2018. Electrolysis of iron in a molten oxide electrolyte. *Journal of Applied Electrochemistry*, 48:115–126.

Yuan, B and Haarberg, G.M, 2009. Electrowinning of Iron in Aqueous Alkaline Solution Using Rotating Disk Electrode. *Rev. Met. Paris*, 106(10):455-459.

Zhou, Z, Jiao, H, Tu, J, Zhu, J and Jiao, S, 2017a. Direct Production of Fe and Fe-Ni Alloy via Molten Oxides Electrolysis. *Journal of The Electrochemical Society*, 164(6):E113-E116.

Zhou, Z, Wang, S, Jiao, H and Jiao, S. 2017b. The Feasibility of Electrolytic Preparation of Fe-Ni-Cr Alloy in Molten Oxides System. *Journal of The Electrochemical Society*, 164(14):D964-D968.